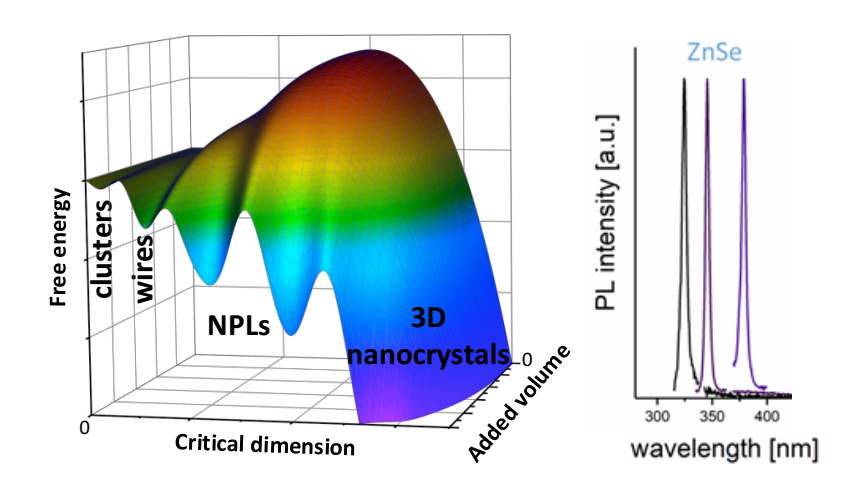
Quantized Reaction Pathways for Solution Synthesis of Colloidal ZnSe Nanostructures: A Connection between Clusters, Nanowires, and Two-Dimensional Nanoplatelets

Patrick D. Cunningham,¹ Igor Coropceanu,¹ Kavan Mulloy,¹ Wooje Cho¹, and Dmitri V. Talapin^{1,2}*

TOC Graphical abstract



¹ Department of Chemistry and James Franck Institute, University of Chicago, Chicago, Illinois, 60637, USA

² Center for Nanoscale Materials, Argonne National Laboratory, Argonne, IL 60439, USA

^{*}E-mail: dvtalapin@uchicago.edu

Abstract

The morphology of nanocrystals serves as a powerful handle to modulate their functional properties. For semiconducting nanostructures, the shape is no less important than the size and composition in terms of determining the electronic structures. For example, in the case of nanoplatelets (NPLs), their 2D electronic structure and atomic precision along the axis of quantum confinement makes them well-suited as pure color emitters and optical gain media. In this study we describe synthetic efforts to develop ZnSe NPLs emitting in the ultraviolet part of the spectrum. We focus on two populations of NPLs, the first having a sharp absorption onset at 345 nm and a previously unreported species with an absorption onset at 380 nm. Interestingly we observe that the nanoplatelets are one step in a quantized reaction pathway that starts with (0D) magic sized clusters, then proceeds through the formation of (1D) nanowires towards the (2D) "345 nm" species of NPLs, which finally interconvert into the "380 nm" NPL species. We seek to rationalize this evolution of the morphology in terms of a general free energy landscape, which under reaction control allows for the isolation of well-defined structures, while thermodynamic control leads to the formation of 3D nanocrystals.

Keywords: nanoplatelet, ZnSe, 2D, nucleation, dimensionality

Colloidal nanocrystals (NCs) can now be synthesized with impressive size and shape control.¹ A wide variety of anisotropic growth methods can be utilized, such as templated growth ², natural tendency of some phases toward anisotropic growth³, or the growth directed by facet specific surface-ligand binding.^{4, 5} Advances in synthetic shape control have led to a variety of colloidal nanomaterials, some with atomically precise dimensions. The classic example of such structures are two-dimensional (2D) CdSe nanoplatelets (NPLs)⁶ with the electronic structures of quantum wells,⁷ extremely narrow photoluminescence (PL) linewidth with quantum yields above 80%,⁸ and directional light emission,^{9, 10} and low lasing threshold,¹¹ and giant optical gain coefficients.¹² Atomically precise NPL emitters are not only attractive for their high color purity and quantum yield—the strongly directional emission is expected to significantly enhance the outcoupling efficiency in light-emitting diode (LED) structures.^{13, 14}

Several distinct formation mechanisms have been proposed for the solution-synthesized 2D nanomaterials. Quasi-2D CdSe NPLs,^{7, 15, 16} nanoribbons,^{17, 18} nanosheets,¹⁹ and quantum belts^{20, 21} are observed to form under various reaction conditions. These structures are formed under two distinct synthetic categories, one using long-chain amine solvents at lower temperatures, yielding wurtzite structures, and the other in the presence of carboxylic acids at higher temperatures, yielding zinc-blende structures.²²

The mechanism of 2D wurtzite CdSe formation was first hypothesized as growth inside soft colloidal templates.¹⁹ The amine-bilayer template, formed *via* dissolution of metal salt precursor in long-chain amines, is known to have lamellar structure and is hypothesized to be a planar reaction gallery in which 2D nanocrystals nucleate and grow.^{19,23} The exact role of the template is unclear, as the presence of lamellar stacks observed *ex situ* has been claimed to be evidence of template-controlled reaction. Additionally, it is suggested that this template plays a role in either stabilizing assemblies or directing nucleation of "magic-sized clusters" (MSCs).^{2, 15, 20} Recent work suggests MSCs can be formed upon introduction of chalcogenide precursor in an isotropic/amorphous mixture containing metal ions, surfactants, and solvent with lamellar mesophases subsequently forming and acting as a stabilizing environment.^{24, 25}

Likewise, Riedinger *et al.* recently proposed an alternative mechanism where 2D growth occurred in isotropic medium as a result of a kinetic effect favoring nucleation and growth of a 2D rather than 3D crystal, yielding different populations of quasi-2D NPLs with zinc-blende structure.²⁶ This growth mechanism does not require a molecular template. Furthermore, the

distribution of populations jumps sequentially between discrete monolayer thicknesses as a function of ripening.^{26, 27} In both wurtzite and zinc-blende CdSe synthetic recipes, it is experimentally observed that small clusters of NCs can transition to 2D structures during synthesis.²⁸ The latter example is especially intriguing as it demonstrates a case of spontaneous symmetry breaking where material with a cubic crystal structure starts to preferentially grow in a 2D manner. Such a process suggests that preformed nuclei can preferentially start growing in one particular plane even in an isotropic solution either through incorporation of free monomers^{26, 29} or through coalescence of existing nuclei.³⁰ This principle has been further demonstrated where small purified zinc-blende spherical CdSe NCs were reintroduced into growth mixture and formed CdSe NPLs through intraparticle ripening and lateral extension.³⁰ An understanding of these pathways is critical to precise control of suitable materials for optoelectronic applications

In contrast with their Cd-based counterparts, Zn-chalcogenides represent a less explored class of materials, despite being an attractive target for heavy-metal-free "green" quantum confined nanostructures. ZnSe, with a bulk band gap of 2.7 eV, is a promising semiconductor emitter for the UV-blue region. The first synthetic routes for emissive ZnSe NCs were reported using reactive diethyl zinc and trioctylphosphine selenium in long chain amines at high temperatures.³¹ Shell-growth of ZnS can be performed to improve the photoluminescence quantum yield of these structures.^{32, 33, 34}

In spite of an early discovery of colloidal routes to ZnSe NCs and their intrinsic polytypism,³⁵ shape control of ZnSe has been somewhat limited compared to Cd-based materials. Early examples of shape control in ZnSe structures utilized injection or addition of precursors in hot alkylamine mixtures to yield nanorods/nanowires in ordered arrays³⁶ or isolable oblate species with some rod-like character.³⁷ In the case of CdSe and CdS, emissive nanorod heterostructures can be precisely controlled by highly selective seeded-growth along the wurtzite *c*-axis.³ These tunable structures have attracted broad interest as a result of their attractive optical properties combining an anisotropic shape with near unity quantum yields.³⁸ A similar level of control and optimization for anisotropic ZnSe nanorods remains elusive. Currently, it is proposed that ZnSe nanorods instead be formed through lower-temperature routes in which nanowires formed in alkylamine bilayer template are truncated and aged.³⁹ This ripening requirement leads to thermodynamic control of their width, with recent improvements in length control realized by tuning synthesis with addition of molecular Zn₄ clusters.⁴⁰

The synthetic routes to quasi-2D ZnSe nanostructures and their corresponding mechanisms of formation are even less explored. ZnSe nanosheets with wurtzite crystal structure have been synthesized in primary alkylamine mixture, with NC oriented attachment proposed as the driving force. The lamellar templated growth of ZnSe NPLs from MSC starting material has been also reported. The absorption spectra of ZnSe MSCs often share the same doublet of sharp absorption maxima as platelets, which obfuscates clear delineation of the transition from 0D to 2D structures probed by UV absorption. For example, three populations of ZnSe MSCs with two absorption peaks and lowest energy excitonic transition at 291 nm, 318 nm, and 345 nm were observed in one-pot syntheses but characterization of 0D, 1D, or 2D morphology from TEM images was ambiguous.

The technological potential of ZnSe NPLs as Cd-free emitters for LEDs prompted us to develop a better understanding of quantized growth mechanism responsible for the formation of distinct populations of ZnSe nanostructures with 2D electronic dimensionality. Unlike low-temperature growth methods for wurtzite CdSe 2D structures, our higher temperature synthesis occurs absent of a liquid template and is likely dependent on the facet-specific nucleation barriers. The experimental data suggest that the formation of ZnSe MSCs, 1D wires and 2D NPLs can be rationalized within the same reaction pathway, with different products forming as a tradeoff between the height of nucleation barrier height and the change of free energy during the following growth. The surface reaction-limited nucleation and growth pathways enable an improved synthetic route towards atomically precise ZnSe nanoplatelets—with the formation of a previously unreported NPL family. These NPL species have narrow UV photoluminescence and can be isolated in high purity. The synthetic and mechanistic information may inform the possible future synthetic routes to high-quality anisotropic nanomaterials for emissive applications.

Results and Discussion

ZnSe nanostructures on quantized-growth pathway. The basic premise of our synthetic study was inspired by the previously reported growth of ZnSe nanosheets using a heat-up approach in the presence of amines. From this starting point we explored the role of Zn and Se precursors, reaction times, and temperatures on the final reaction products. In our main reaction scheme, a zinc precursor (zinc acetate, stearate, nitrate, or oleate) was combined with selenium in an oleylamine/octylamine mixture and the solution was first heated to 100 °C for 30 minutes and

finally to 170 °C (see Methods Section for full details). Under these conditions we found that the reaction exhibits quantized growth that proceeds through four kinetically trapped populations (see Figure 1a for the UV-VIS spectra, and Figure S1 for a schematic representation). Importantly, the populations are observed sequentially—early in the reactions we observed populations with the optical transitions at the highest energy, while the species showing optical transitions at the lowest energy formed at terminal stages of the reaction. We isolated and studied these populations to determine their morphology.

Throughout heat-up synthesis, the first distinct population, with the absorption peak at 291 nm (4.26 eV), formed around 120 °C and isolated as 100-500 nm sized layered structures, also known as mesophases (Figure 1b).²⁴ It is believed that such mesophases can stabilize MSC species by kinetically arresting them against growth.²⁴ The formation of ZnSe clusters has been suggested in the literature and similar optically-precise doublet species have been reported.⁴² It is worth noting that the stability and structure of the layered mesophases that tend to accompany the growth of metal chalcogenide NCs are actively explored areas of research in their own right. Multiple factors have been put forward to account for the formation of such structures, including the role of surfactant/precursor interactions and dipolar interactions between MSCs.^{24, 25} While this topic was not the focus of the present work, we were able to use *in* situ SAXS studies to obtain some insight into the nature of the mesophase relevant to the system we investigated. For example, a key conclusion was that MSCs and subsequent structures did not simply grow in pre-formed metal-amine bilayer templates. Rather, the presence of both Zn and Se precursors in the amine medium was necessary to generate the mesophases observed at high temperatures (>100 °C). These points are discussed in more detail below and in section S-1.

In some syntheses, a distinct population is observed starting at temperatures of approximately 130 °C with first absorption peak at ~318 nm. This species is rarely observed without additional populations present. When isolated, this species appears as long bundles of very thin (~1 nm) wires (Figure 1c). These nanostructures show PL band peaked at 320 nm (3.875 eV), with the full width at half-maximum (FWHM) of 5.0 nm or 60 meV (Figure S12). Such a narrow ensemble emission spectrum is comparable to the width of single-particle emission spectra, which suggests an absence of inhomogeneous broadening typical for a population of ZnSe "quantum wire" species with atomically precise cross-sections. Although it is interesting to consider whether the layered structure of the preceding mesophase played any role in directing the formation of these quasi 1-

D structures, we were not able to obtain any conclusive experimental evidence in this regard. The first observation of clear quasi-2D ZnSe nanostructures appears with first absorption feature at 345 nm, which begins to form near 150 °C. This population generally appears as discrete platelets with rectangular shape (Figure 1d). Finally, we have demonstrated the isolation of another quasi-2D ZnSe nanostructure population with first absorption at ~380 nm, which had never previously been reported. These species are typically isolated as long nanosheets (Figure 1e). All the above 0D, 1D and 2D ZnSe nanostructures can form from the same precursors, with the temperature as the product-defining tuning knob. Fine-tuning of the reaction conditions allows optimization of the reaction yield for different nanostructures.

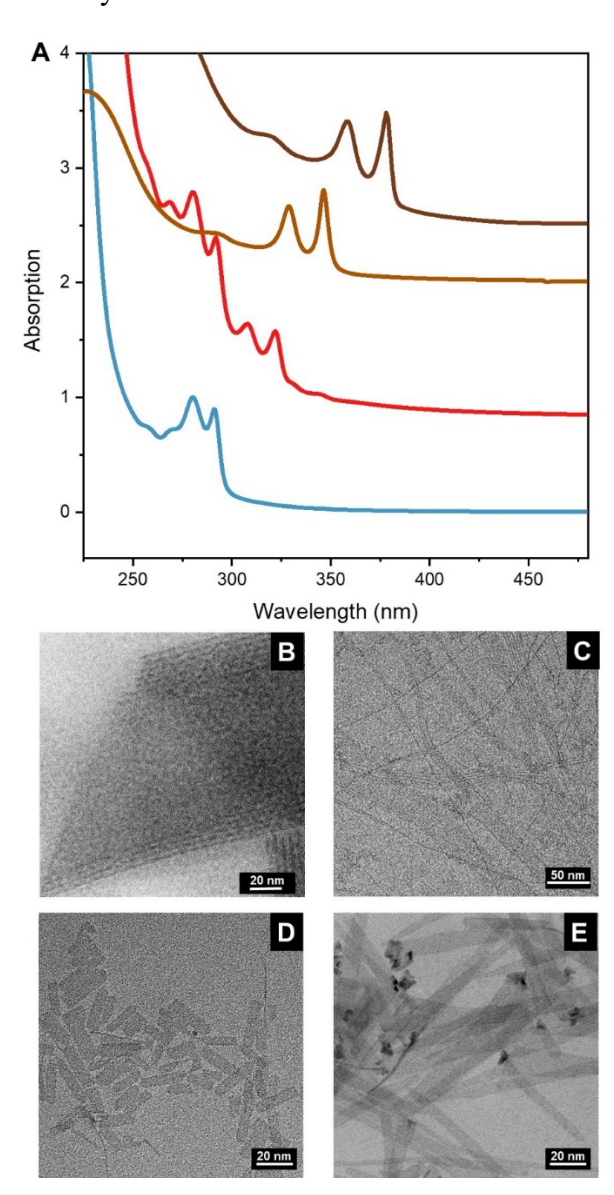


Figure 1. Accessible populations of ZnSe nanostructures synthesized in heat-up protocol: (A) Absorption spectra of all populations isolated and observed at varying stages of 2D nanostructure synthesis. (B-E) TEM images of the relevant isolable species. (B) Sub-micron size triangular mesophases of species with first absorption peak at ~291 nm show lamellar-type structuring. (C) Species with first absorption peak at ~318 nm show long bundles of thin nanowires. (D) Nanoplatelets with first excitonic transition at ~345 nm isolated with discrete platelet morphology. (E) Species at with first excitonic transition at ~380 nm isolated with nanoribbon like morphology.

Isolation and characterization of pure populations of quasi-2D ZnSe nanostructures. A consequence of this quantized-growth pathway is that we have demonstrated two populations of colloidally-stable NPLs with narrow absorption and emission linewidth (Figure 2a-c). The first NPL population showed absorption maximum at 345 nm and band-edge PL with negligible Stokes shift (Figure 2a). The FWHM of the emission band was found to be 4.0 nm (41 meV). The absorption spectra show two sharp peaks, previously observed for 2D-quantum wells of II-VI semiconductors, interpreted as electronic transitions involving the heavy hole and light hole states and the conduction band, all within the first QW sub-band.⁷ Another peak with a lower intensity is observed further to the blue, likely to correspond to the transition from split-off hole state to the conduction band⁷. The platelet thickness was measured through TEM analysis of platelets that were stacked on their side. The thickness of "345 nm" NPLs was measured to be $l_{345} = 1.47 \pm 0.17$ nm (Figure 3A). This is consistent with previously reported value of 1.4 nm.⁴¹ The "345 nm" population has already been assigned to a 4 monolayer (ML) population⁴¹ and we find that the thickness we measure is consistent with a structural model for 4ML wurtzite ZnSe platelets (1.41 nm).

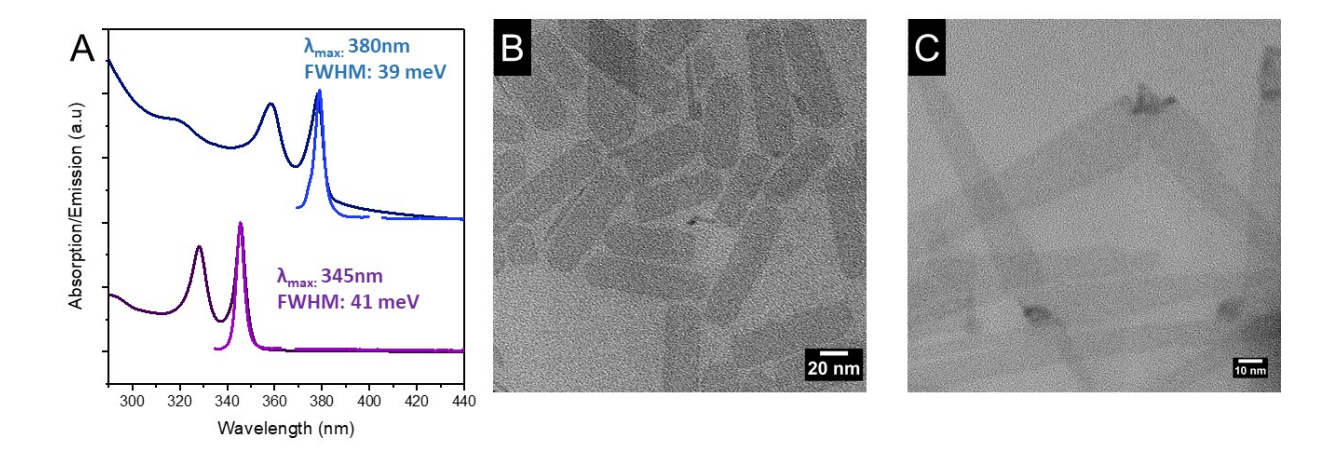


Figure 2. Two populations of discrete quasi-2D ZnSe nanostructures: (A) Absorption and emission spectra of showing extremely narrow linewidth in the UV. TEM images showing morphology of species with (B) absorption at 345 nm and species with (C) absorption at 380 nm.

Under certain conditions, the "345 nm" platelets undergo a well-defined transition to a new population. This transformation occurs either when using high concentrations of reagents (a concentration greater than 100 mM for the limiting reagent) or when elemental selenium is added after the 345 nm population forms. The new NPL population shows the first absorption maximum at 380 nm, and PL emission band with the FWHM of 4.4 nm (39 meV) (Figure 2a). The thickness of "380 nm" NPLs was measured by TEM as $l_{380} = 1.84 \pm 0.20$ nm (Figure 3B).

Interestingly, the "380 nm" population appears to not only have a larger thickness, but XRD studies strongly indicate that it also has a different crystal structure (see Fig. 3C). In the case of "345" NPLs, the wurtzite X-ray reflections were very clear with enhanced (002) peak and suppressed (110) and (112) (Figure 3, black). In contrast, in purified samples of "380 nm" NPLs, we consistently see peaks that are characteristic of cubic zinc-blende (zb) structure (Figure 3C, red). No strong reflections from (102) and (103) planes are observed, which is in line with the previous studies of zb-CdSe NPLs. ⁴⁴ A small shoulder at ~26 degrees may correspond to the (100) peak from a minor impurity wurtzite component. The observation of a phase change is supportive of separate nucleation and subsequent growth modes of "380 nm" NPL structures as discussed below. This apparent phase change supports the mechanism we describe below, where "380 nm" NPLs grow from different zinc-blende nuclei and do not simply grow through the addition of

monolayer on an existing large "345 nm" NPL. Another interesting feature of the "380 nm" NPLs is that HRTEM indicates that the wide facet appears to belong to the {110} family (see Figure S12), unlike typical zb-CdSe platelets terminated with {100} type facets. The thickness of the platelets would then be consistent with 4.5 unit cells of zb-ZnSe oriented in the [110] direction along the short axis.

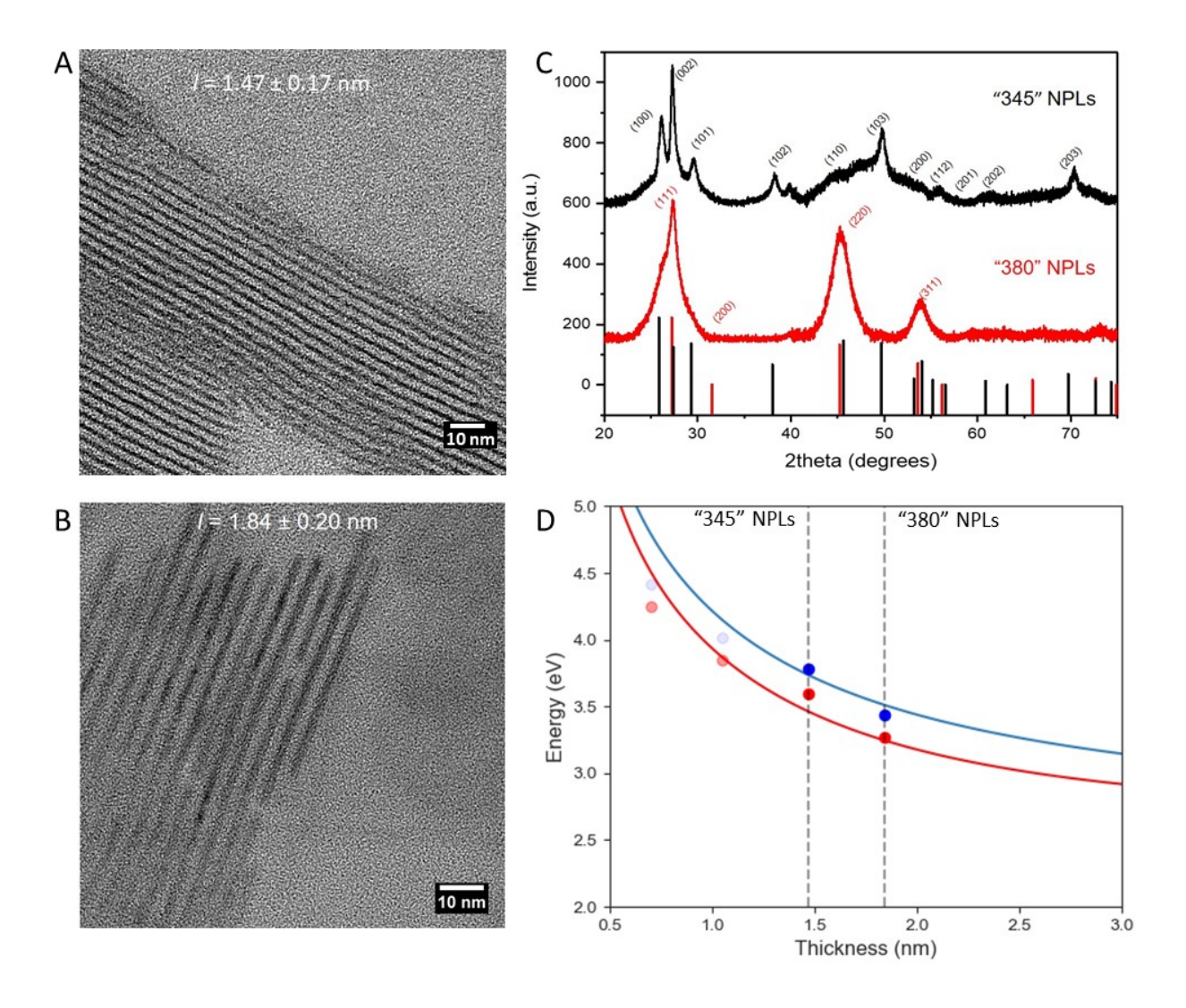


Figure 3. Structural characterization of the NPL populations. (A, B) TEM analysis of controlled stacks of each platelet population prepared by flocculation from methylcyclohexane/ethanol. (C) Powder X-ray diffraction patterns of "345 nm" ZnSe NPLs (black) and "380 nm" ZnSe NPLs (red) compared with the bulk reflections for wurtzite and zn-blende ZnSe phase, respectively. (D) Band energy of heavy hole (red trace) and light hole (blue trace) calculated using eight-band Pidgeon-

Brown Hamiltonian to a 2D system bounded by infinite potential barriers. Calculated values are plotted against experimental values for peaks observed from the absorption features (based on the experimentally determined thicknesses of the 345 nm and 380 nm NPLs). The thickness values for the two highest energy species are calculated under the assumption that they are 2 and 3 monolayer wurtzite species, but unsurprisingly they produce a poor fit given the fact that they are not 2D structures.

The experimental energies for the first and the second excitonic transitions in "345 nm" and "380 nm" ZnSe NPLs have been compared to the calculations using an effective mass model for quantum well structures (Figure 3d). In order to estimate the excitonic energy levels in ZnSe nanoplatelets we have taken the approach first described by Efros *et al.*⁷ Briefly, the position of the bulk bands is calculated within an effective mass formalism based on the application of the eight-band Pidgeon-Brown Hamiltonian to a 2D system bounded by an infinite potential barrier. Additional details on the calculation are provided in Supporting Information. A good agreement was found between the experimentally measured optical transition energies and calculated values for the "345 nm" and "380 nm" ZnSe NPLs.

On the mechanism of formation for "345 nm" ZnSe NPLs. Previous works have suggested that anisotropically structured metal-amine precursor serves as a "soft-colloidal template". This template plays the key role in directing the growth of flat wurtzite (w) metal-chalcogenide NPLs. 19, 20, 23 In the case of ZnSe, the literature indicates that NPLs could be formed from MSCs trapped within soft-template mesophase. The early species generated in our synthetic protocols show the first absorption peak at 291 nm and resemble MSCs with nearly identical absorption peaks to those reported in the literature. Unfortunately, the absence of published single-crystal data for these MSCs does not allow us to fully rule out alternative explanations. In our work, "291 nm" ZnSe nanostructures assigned to MSCs are coordinated in lamellar mesophases in the early stages of synthesis (Figure 1b), pointing to the possible role the mesophase as growth-directing agent.

As an alternative model, the Norris group developed a model for the growth and stability of various populations of zb-CdSe NPLs. 26, 27 Their model and experimental data suggest that the growth of zb-CdSe NPLs are not dependent on a template, but rather governed by differences in facet-specific growth determined by the island nucleation kinetics.

Here we sought to reconcile the growth of our ZnSe NPLs with either one or both of these models by assessing different stages of NPL formation. The time-evolution of the absorption spectra was used to analyze and isolate the intermediate species and identify critical temperature points. At early stages of the reaction, quantitative formation of the "291 nm" species is observed when the reaction is held at 100 or 125 °C (Figures 4a and 4b). These intermediate aliquots are solution-soluble mesophases that stabilize some form of atomically precise species (Figure 4b). Extended reaction times finalize the transition of "291 nm" species into "345 nm" w-ZnSe with first optical transition at 345 nm (Figure 4a-b). In aliquots containing both sets of species, we observed the presence of both 100-500 nm sized mesophases and free-standing NPLs (Figure S2). This observation likely indicates that species stabilized within these mesophases can supply reactants for "345 nm" platelets through dissolution. The difference in size and shape of platelets versus mesophases called into question the presence of an annealing process of platelets within the colloidal template as planar reaction gallery. Thus, the state of the metal-amine precursor at high temperatures was determined using small-angle X-ray scattering experiments (SAXS). Concentrated templates of the relevant amines (oleylamine and octylamine) within the reaction mixture were prepared and added to capillaries where they were subject to slow-heating. Both zinc-amine complexes had lamellar structure with a set of (00*l*) peaks that scaled with the length of the amine chain (Figure 5c, Figure S3a). Interestingly, the sharp lamellar peaks disappear into broad peaks at temperatures less than or equal to 60 °C, indicating that lamellae templates completely disappear and form a glassy/disordered state of the Zn-amine complex (Figure 4c). Further analysis shows that this transition from lamellae to isotropic phase to be general for a variety of solvent mixtures and concentrations (Figures S3-S5). We therefore conclude that it is highly unlikely that lamellar template plays any role in the formation of "345 nm" w-ZnSe NPLs exhibiting the emission peak at 345 nm.

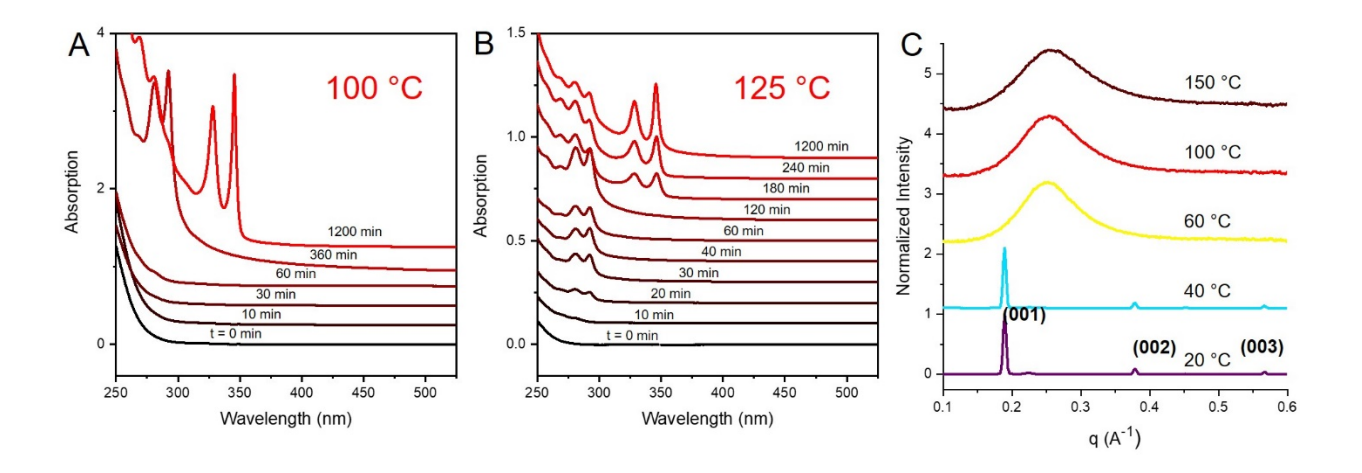


Figure 4. Nanoplatelet species form at temperatures which lack a metal-amine lamellar reaction template: (A-B) Temporal evolution of atomically precise species in absorption spectra after heating reaction mixture to (A) 100 °C and (B) 125 °C. (C) X-ray scattering experiments revealing that lamellar-structured Zn-oleylamine complexes become isotropic at relevant reaction temperatures (>60 °C).

Sequential ripening from "345 nm" NPLs to "380 nm" ZnSe NPLs. As we increase reaction temperature, the formation of "345 nm" platelets accelerates (cf. Figures 4a and 4b). Interestingly, when a high concentration of the zinc and selenium precursors is maintained (at concentrations greater than 100 mM for the limiting reagent), we see a transition to "380 nm" NPL species (see the Methods Section for complete details). For this system, the time evolution of the absorption spectra reveals that 291 nm species are formed and then a high concentration of "345 nm" species is rapidly observed upon heating to 150 °C (Figure 5a). Once saturation of "345 nm" species is reached, we begin to see the formation of "380 nm" species until they are the only species present after 20 hours (Figure 5a). Similar to the model recently proposed for sequential ripening of NPLs (and earlier in the case of spherical clusters⁴⁵),²⁷ a stage of the reaction is observed where the normalized absorption of "345 nm" and "380 nm" NPL species is in steady-state (Figure 5b). This stage is believed to be in the regime where "380 nm" species have nucleated from dissolving "345 nm" species and where rate of lateral growth for the "345 nm" species is equal to the rate of dissolution to generate new species. This effect can be observed through TEM of the aliquots along this stage of the reaction (Figure 5c). Interestingly, these images show increasing lateral growth

with increasing presence of species which have a morphology indicative of "380 nm" quasi-2D NPL structures. These observations support interpretation of the quantized growth of ZnSe NPLs as a surface-reaction limited pathway where the formation of initial atomically precise species governs the thermodynamic ripening process into subsequent populations. Kinetic studies of heat-up synthesis to even higher temperatures, *e.g.*, 175 °C, reveal evidence that we bypass the critical temperature for reduced dimensionality nucleation and eventually destroy the sharp features in the absorption spectra (Figure S6a), characteristic of polydisperse colloidal ZnSe nanoparticles. Unsurprisingly, in TEM we see a mixture of nanocrystals, rods and wires with negligible platelet morphology present (Figure S6b). The pathway to metastable "380 nm" NPL population is likely bypassed at these temperatures such that when the next sequential set of nuclei form, the reaction falls under a 3D growth pathway.

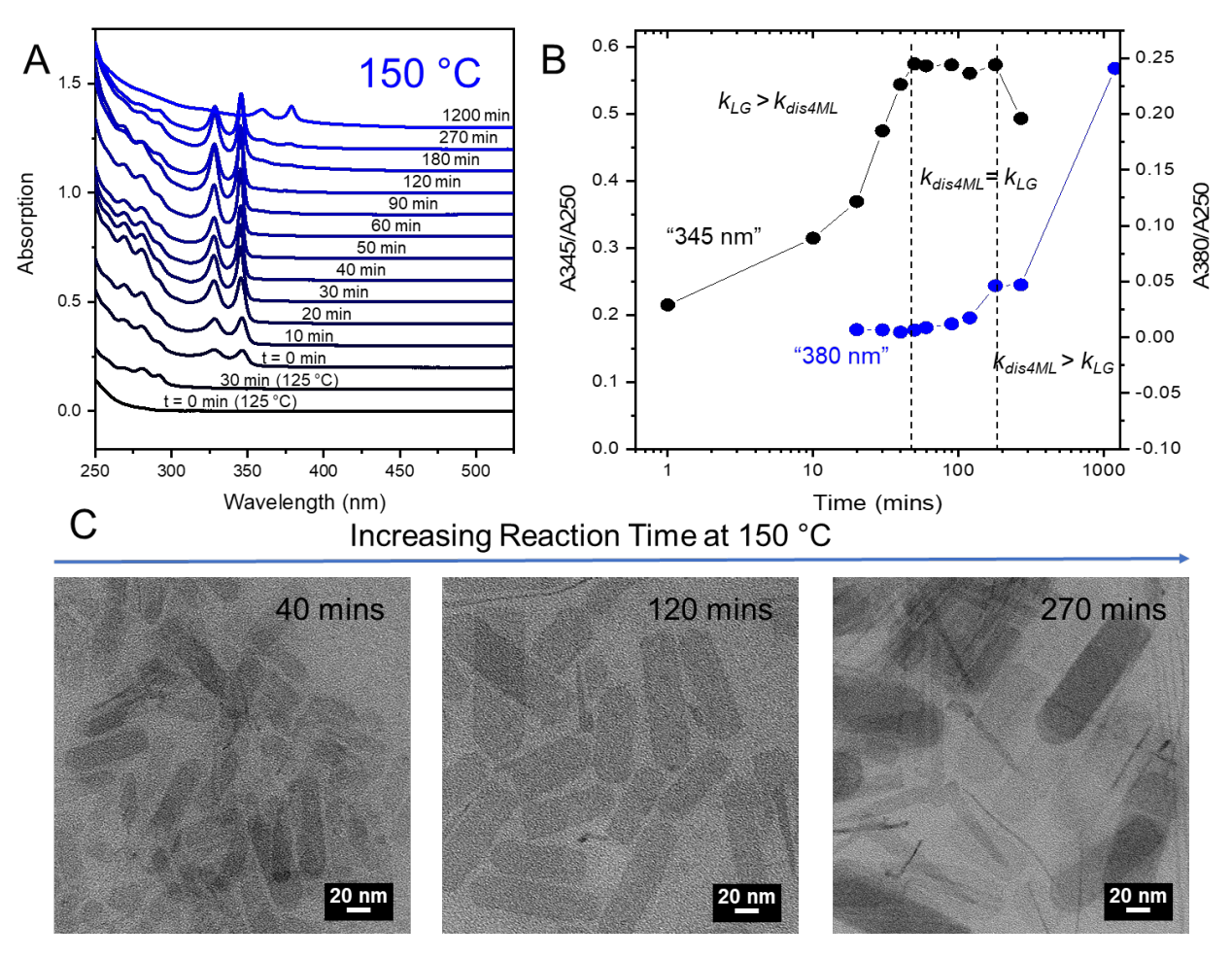


Figure 5. High temperature lateral growth and sequential ripening of "345 nm" ZnSe platelets: (A) Temporal evolution of atomically precise species in the absorption spectra. (B) Analysis of

absorption features for "345 nm" and "380 nm" NPL populations normalized to their absorption at 250 nm with respect to reaction time. (C) TEM analysis of populations containing both sets of NPL species demonstrates lateral platelet growth and increased presence of new species.

Considerations on the role of dimensionality in NC nucleation and growth. In most colloidal syntheses, NCs tend to grow isotropically to minimize surface-to-volume ratio, forming nearly spherical particles. As a consequence, the synthetic conditions that favor anisotropic shapes are often quite different from those that produce spheres. Starting with a solvent-surfactant consisting of primary amine(s), we can combine $Zn(X)_2$ salts (X = oleate, stearate, acetate, nitrate, or chloride) and elemental Se to generally yield ZnSe nanostructures (Figure 6a). At the molecular level, elemental Se reacts with primary amine RCH_2NH_2 forming selenoacylamide $RC(Se)NH_2$, which transfers the chalcogen to an electrophilic metal ion.⁴⁶

Interestingly, we found that the final material isolated from the reaction mixture varies widely depending on the chemicals addition and growth temperature. Using identical zinc and selenium precursors in primary amine solvents, ZnSe nanostructures with 1, 2, and 3-dimensional confinement can be accessed by biasing the reaction pathway with different reaction temperatures. Analysis of isolated products from reactions shows that we can achieve different species with identical reagents by simply changing the temperature parameters. Combining a zinc salt (zinc acetate or zinc stearate) and elemental selenium in hot oleylamine at 250 °C yields quasi-spherical particles, with some shape irregularities and an impurity of polypod structures (Figure 6b). When precursors are combined at very high temperatures (250 °C and higher) or allowed to rapidly heat, the growth proceeds fast and continuously, leading to mostly isotropic particles that undergo coalescence or ripening. By contrast, when the same precursors are combined at room temperature in primary amines and heated to ~130 °C, 1D ZnSe nanowires (NWs) can be isolated (Figure 6c). Finally, when the same reaction that yields the NWs is heated past 160 °C, 2D ZnSe NPLs are isolated (Figure 6d). In most cases, "291 nm" species, assigned to ZnSe MSCs, preceded the formation of 1D or 2D nanostructures.

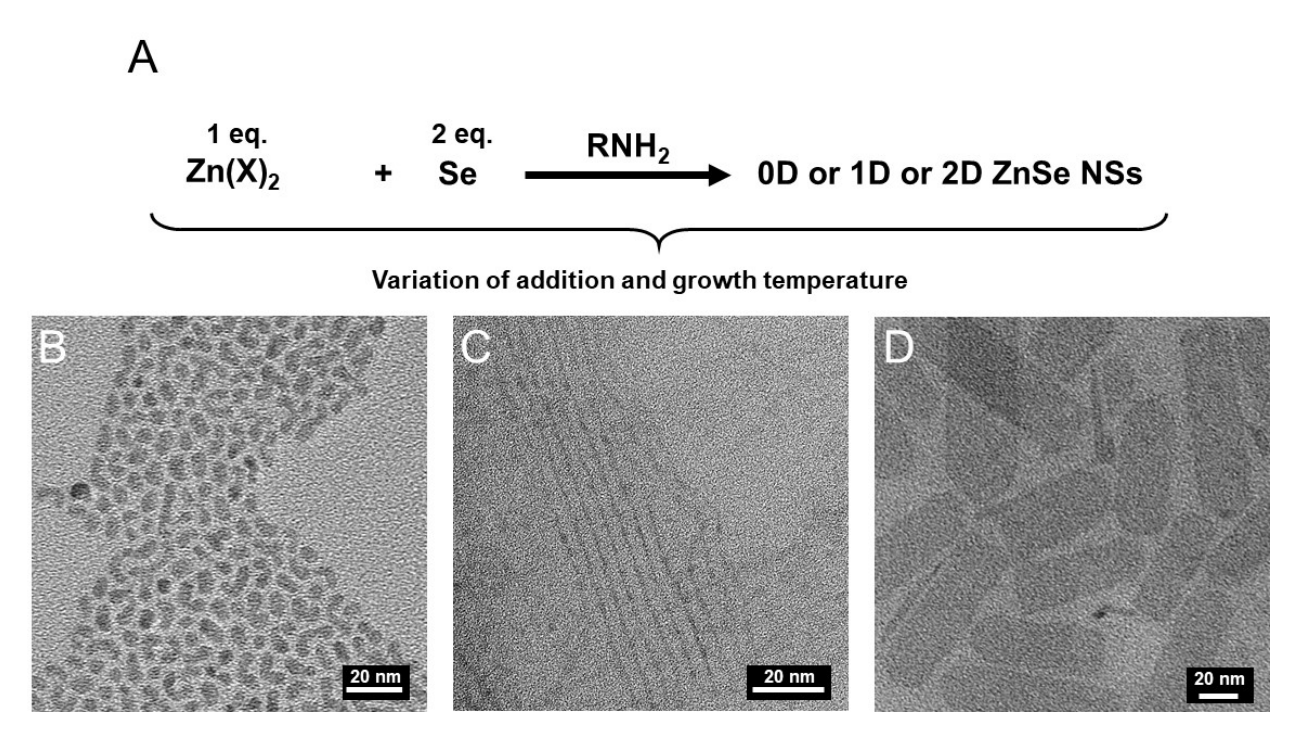


Figure 6. ZnSe nanocrystals of different dimensionality formed starting from same precursors: (A) A generalized reaction scheme of ZnSe nanostructure formation. Variation of addition and growth temperature of one or both monomers determine dimensionality. In all cases zinc stearate was used as the zinc precursor. Oleylamine was used as the solvent for the reaction that produced the structures shown in panel B while a mixture oleylamine and octylamine was used to generate the products shown in panels C and D. The resulting TEM images show the products of these different pathways in the form of (B) (partially sintered) isotropic dots, (C) nanowires, (D) nanoplatelets.

In the classical nucleation theory (CNT), precursors must overcome an activation barrier, where critical nucleus size is reached and further growth occurs continuously. If reagents are mixed rapidly at a high temperature, *e.g.*, in the hot-injection synthesis⁴⁷, the initial formation of reactive intermediates (monomers) and subsequent nucleation are mainly limited by the mixing time of the reagents. The nucleation barrier is overcome and rapid consumption of monomer drives continuous nanocrystal growth (Figure 2). The growth kinetics often falls under diffusion-controlled transport of monomers towards the surface of growing nanoparticles,⁴⁸ that generally favors isotropic growth.²⁶

By contrast, in a quantized growth regime, the nucleus undergoes a series of transformations between shallow metastable potential energy wells. For example, sequential formation of several populations of CdSe clusters has been observed upon gentle heating of the reaction mixture followed by nucleation and continuous growth of nanocrystal phase.⁴⁹ Similar magic sized clusters have been reported for ZnSe as well,^{42, 50, 51} although these have not been studied as extensively as the corresponding CdSe structures.

Our experimental results show that ZnSe MSCs, nanowires, NPLs and nanocrystals all can be realized using identical reagents. Such a diversity of reaction products originated from same starting materials made us to hypothesize the possibility of a unified reaction pathway which, depending on available thermal energy, can multi furcate into a cluster, wire, platelet or bulk crystal growth. Such a regime of quantized growth can occur if the barrier to isotropic nucleation is prohibitively high, and reaction is forced to proceed towards metastable products along pathways with lower nucleation barriers.

Here we propose the general form of free-energy landscape for nanocrystal nucleation and growth as schematically shown in Figure 7. The generalized reaction coordinate is represented by two variables: critical dimension (d) and added volume (V_{add}). The critical dimension represents the smallest dimension for a given shape – diameter for clusters, wires and spherical nanocrystals, and thickness for NPLs. It is related to the smallest possible nucleation volume for given population of species, expressed as $V_N = \pi d^3/6$. In quantum-confined semiconductors, d also determines the band gap and emission wavelength. The added volume is the total volume of the reaction product, V_{tot} , added to extend V_N into 1D wire, 2D sheet or larger 3D crystal: V_{add} = $V_{tot} - V_N$. With exception of the early post-nucleation stage, we can simplify $V_{add} \approx V_{tot}$ and use V_{add} as a measure of the reaction progress, directly related to the fraction of limiting reagent consumed. This approach allows representing colloidal syntheses as trajectories on the potential energy surface leading to various reaction products (Figure 7). The full energy landscape can be complicated, for example, by additional minima formed by a multitude of closed-shell structures, such as MSCs,52 and activation barriers associated with ligands desorption and reorganization. In the following discussion, we ignore these complications and focus exclusively on the factors affecting dimensionality of reaction products.

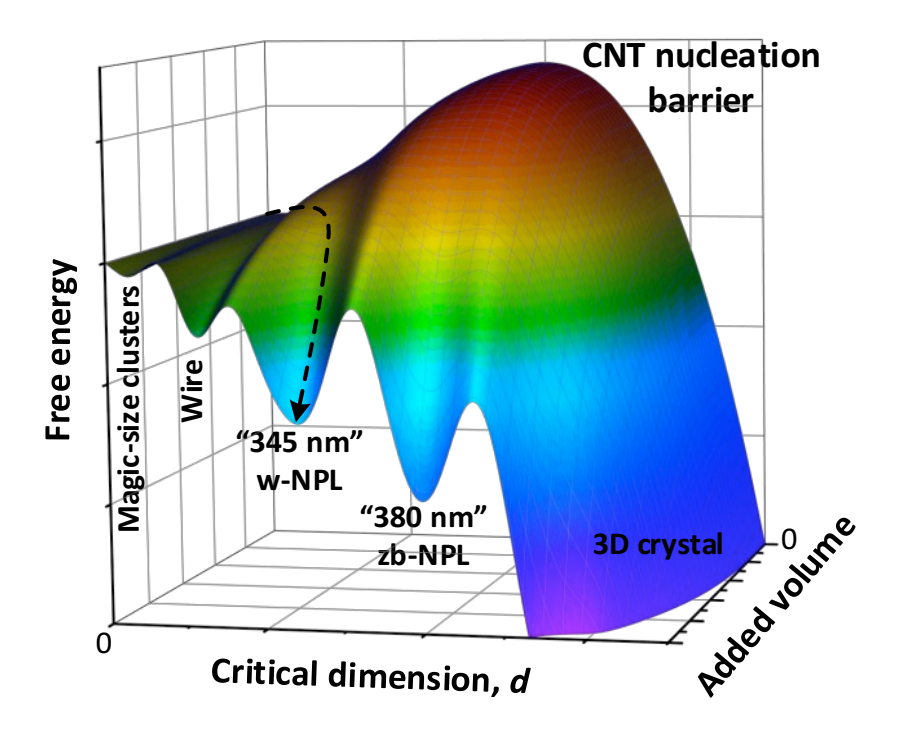


Figure 7. The potential energy landscape for the formation of structures of different dimensionality starting from molecular precursors that proceed through an intermediate magic sized cluster and then proceed through 1D, 2D, or 3D pathways with a characteristic evolution of the free energy. An example of the reaction trajectory leading to "345 nm" ZnSe NPLs is shown by the dashed arrow.

The reaction trajectories can be qualitatively rationalized by considering changes of the chemical potential associated with the nucleation and growth steps. The free energy of the critical nucleus reflects a balance between a favorable energy of formation proportional to the volume and a destabilizing surface energy term that depends on the surface area. CNT predicts that the activation barrier for nucleation depends strongly on system dimensionality.^{53, 54} The shape of nucleation barriers is shown Figure 8a for the 1D, 2D, and 3D cases. Somewhat counterintuitive, the formation of 1D wire does not involve any activation barrier, which has also been seen experimentally.⁵⁴ The nucleation of 2D NPLs has been recently studied in Ref,²⁶ with a conclusion that up to certain critical thickness, the homogeneous nucleation barrier for 2D crystals is smaller

than the barrier for 3D crystal growth (see details in Supp Info section S-2.). The nucleation barrier clearly favors the formation of 1D wires over 2D NPLs, with the nucleation of 3D crystallites being least favorable (Figure 8a). The reaction mixture needs an excess of thermal energy to overcome the nucleation barrier toward isotropic 3D growth.

Once a certain critical nucleus is available, the system can relax in energy by continuing to grow. Importantly, the degree of stabilization experienced upon growth (as a function of V_{add}) will depend strongly on the specific structure of the dominant species. Figure 8b compares the evolution of chemical potential of different nanostructures. The first species observed is an apparent population of MSCs. Because the clusters have a fixed structure, as the reaction proceeds only the total number of clusters can increase, but not their average size or surface-to-volume ratio. As a result, there is only a small energetic stabilization that is simply proportional to the number of clusters formed. At higher temperatures conditions become favorable for the formation of 1D wires, which can grow indefinitely along one dimension, thus providing stability as the reaction proceeds. At even higher temperatures an even greater activation barrier can be surpassed leading to the formation of 2D platelet species. As the species grow laterally, the energy is quickly reduced (as shown by the steeper slope of the curve projected on the free energy $vs.\ V_{add}$ plane). Moreover, thicker platelets require a larger initial input of energy but also relax in energy more rapidly as they grow, making them thermodynamically favorable compared to the thinner species. Finally, as the temperature grows even further the thermal energy is sufficient to erase surface selectivity and finally the system can move past the highest activation barrier to allow for isotropic 3D growth, which results in the steepest slope because of the smallest surface-to-volume ratio. The quantizedgrowth pathway for ZnSe nanostructures can therefore be rationalized as an interplay of the homogeneous nucleation barrier in the free energy vs. d plane and the slope of the potential energy landscape along the free energy $vs. V_{add}$ axis for a given population of MSC, wires, NPLs or larger isotropic nanocrystals. Our analysis suggests all the apparent complexity of the nanoscale morphologies may originate from the generic energy landscape outlined in Figure 8.

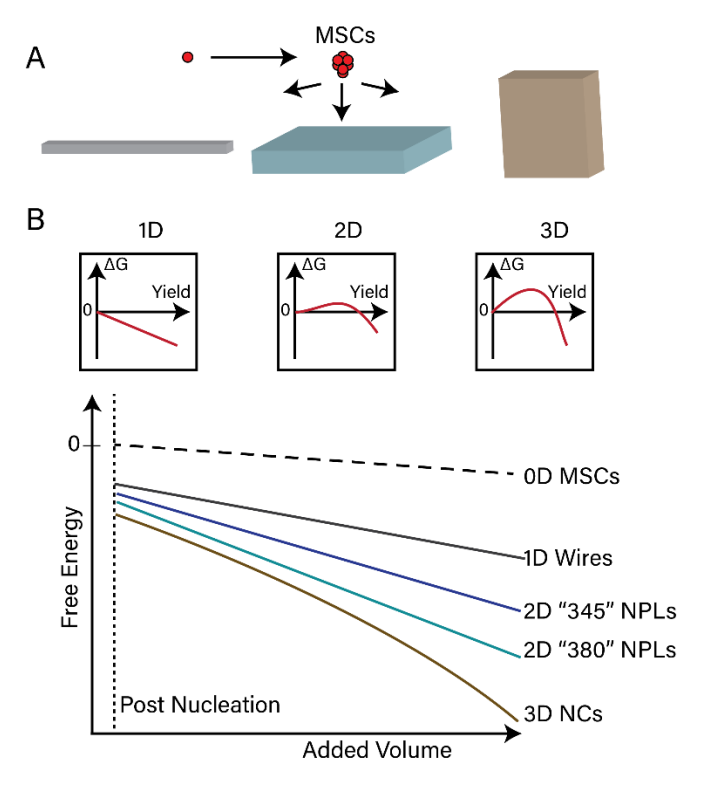


Figure 8. (A) Qualitative comparison of the change in free energy associated with nucleation of the 1D, 2D, and 3D structures. (B) The change in chemical potential associated with the post-nucleation growth for nanostructures of different dimensionality (0D magic sized clusters MSCs, 1D nanowires, 2D "345 nm" and "380 nm" nanoplatelets and spherical QDs).

Conclusions

Using the same simple set of precursors, ZnSe nanostructures of varying dimensionality can be grown depending on differences in the temperature profiles of the reaction. In the lower temperature modes of the reaction pathway, quantized growth is observed and the kinetically trapped products can be isolated as micron-sized mesophases, wires, and two species of quasi-2D nanostructures. In this work, we determined that growth and ripening processes are controlled by a surface-reaction-limited pathway in the range of 100-170 °C. This growth occurs absent a template and quasi-2D nanostructures are observed as part of a complex reaction coordinate in which the likely thermodynamic end product is bulk ZnSe. The discrete 2D nanostructures have narrow PL linewidth and can be added to the available group of NPL emitters that may demonstrate

potential for display and lighting applications. Understanding of the growth mechanism is crucial to the optimization of their synthesis and optical properties tailored towards these applications.

Methods

Chemicals. Zinc nitrate (99.9 %, Sigma-Aldrich), zinc chloride (99 % Sigma-Aldrich), zinc acetate (99.9 %, Sigma Aldrich), zinc stearate (99 %, Sigma Aldrich), selenium powder (9.9% 100 mesh, Strem), octylamine (99 %, Sigma-Aldrich), methylcyclohexane (Sigma Aldrich), ethanol (Fisher Scientific), ethyl acetate (Fisher Scientific), were used as obtained. Oleylamine (70 %, Sigma-Aldrich), was often dried at 120 °C and stored in the glove box before extensive use. Zinc oleate was prepared using a modified method from the literature. In short, oleic acid (90 %, Sigma-Aldrich) was dried and stored in the glove box. To a 250 mL 3 neck round bottom flask containing 100 mL of pentane, 9 grams of dried oleic acid was added. The flask was transfer to a Schlenk line under N2 atmosphere and maintained under an ice bath. To the oleic acid solution with extreme caution, 17 mL of a 1.0 M solution of diethyl zinc in hexane (Sigma Aldrich) was added under stirring. After addition the ice bath was removed and allowed to stir overnight. Upon obtaining a white suspension in solution, the flask was transferred to a glovebox and collected in a vacuum frit and washed with hexane/pentane. The isolated zinc oleate was further vacuum dried in a 40 mL vial and stored in the glovebox.

ZnSe Magic-Sized Clusters, Nanowires, and Nanoplatelets "345 nm" ZnSe nanoplatelets

This population of nanoplatelets was grown in a similar manner to a literature recipe with several modifications.⁴¹ To a 100 mL three-neck round bottom flask, 187 mg (0.3 mmol) of zinc stearate was added along with 10 mL of oleylamine. The flask was heated under vacuum at 100 °C for 90 mins before cooling back to room temperature under nitrogen. To the cooled flask, 5 mL of octylamine and 48 mg of selenium powder (0.6 mmol) was added under positive N₂ pressure and resealed. After evacuating and refilling with N₂ several times, the flask was heated to 100 °C and allowed to rest for 30 mins. The flask was then heated to 170 °C, taking special care to make sure

the temperature does not exceed 170 °C. The platelets proceeded with growth at 170 °C for anywhere from 5 mins to 6 hours. The generality of this approach was extended to several different ranges of temperatures, reagents, and concentrations. After completion, the mixture was cooled naturally and 2 mL of *n*-trioctylphosphine (TOP) was added to the flask at ~70 °C to quench any unreacted Se species. The resulting turbid white suspension was then transferred to a glovebox and precipitated *via* centrifugation. The precipitate was then redispersed in ~15 mL of methylcyclohexane at which time any insoluble side products or nanoparticles were precipitated by centrifugation without non-solvent. The supernatants contained concentrated NPL solutions and can be further purified using a small amount of ethanol before or after storage.

Magic Sized Clusters and Nanowires

Magic sized clusters and nanowries were prepared in exactly the same manner as the "345 nm" NPLs described above with the difference that instead of heating up the solution to 170 °C, it was only heated up to 120 °C in the case of the magic sized clusters and 130 °C in the case of the nanowires. It should be noted that isolation of these two populations generally proved more difficult, since the evolution from MSCs to nanowires occurred tended to occur very rapidly (on the order of only a few minutes), such that aliquots taken from the reaction often contained a mixture of the two species in different proportions.

"380 nm" ZnSe nanoplatelets. Thicker, atomically precise platelets with first absorption at 380 nm can be synthesized using a simple modification to the above procedure for "345 nm" platelets. After heating the flask to 170 °C, the reaction is allowed to proceed for 20 mins. At this time, an excess of Se shot (100-200 mg) is added to the reaction flask to make available more soluble precursor. This addition induces a transition to a lower energy atomically-precise nanoplatelet—in order to ensure quantitative transition, the absorption was monitored with needle-tip aliquots injected into 5% TOP in methylcyclohexane every 10 mins until the peak at 345 nm disappeared. This transition typically takes 30-120 mins and it was also found that we could achieve partial transitions with more rapid increase of temperature and deliberate overshoot to 180 °C. However, care should be taken to avoid the formation of larger polymorphic-species that often form as a result of this transition. Full transitions could also be achieved with higher concentrations of starting reagent and longer reaction times, which will be discussed in future ripening experiments.

Ripening experiments. Instead of addition of Se shot, we used a larger concentration of precursor

(200 mM Zn, 400 mM Se) in order to analyze the temporal evolution of platelet species. Zinc

oleate was used in order to ensure complete dissolution of zinc precursor to leave the saturation of

selenium as the only uncontrolled variable. In the high concentration synthesis, we expect to

maintain a reservoir of precursor and monomer and could examine the evolution of each species

as reactions were held at constant temperature (100, 125, 150, or 175 °C) in order to reveal the

kinetic aspects of the reaction mixture. The absorption was monitored with needle-tip aliquots

injected into 5 % TOP in methylcyclohexane and representative samples were analysis in TEM.

Characterization techniques. Absorption spectra of ZnSe samples in dilute solutions of

methylcyclohexane were measured using a Cary5000 UV/Vis Spectrophotometer.

Photoluminescence spectra were collected using a Horiba JobinYvon Fluoromax-4. Transmission

electron microscopy (TEM) was done using a Technai F30 and a Technai Spirit.

The SAXS patterns of capillaries were collected on SAXSLab Ganesha instrument with Cu Ka

radiation.

ASSOCIATED CONTENT

Supporting Information

Additional experimental details, SAXS curves, TEM images. This material is available free of

charge *via* the Internet at http://pubs.acs.org."

The authors declare no competing financial interests.

AUTHOR INFORMATION

Corresponding Author

dvtalapin@uchicago.edu

23

ACKNOWLEDGMENT

This work was supported by the Samsung GRO Program, National Science Foundation under award number DMR-1905290, by the Office of Basic Energy Sciences, the US Department of Energy (grant no. DE-SC0019375), by the Department of Defense (DOD) Air Force Office of Scientific Research under grant number FA9550-15-1-0099. This research used resources of the Center for Nanoscale Materials, a U.S. Department of Energy (DOE) Office of Science User Facility operated for the DOE Office of Science by Argonne National Laboratory under Contract No. DE-AC02-06CH11357.

REFERENCES

- 1. Yin, Y.; Alivisatos, A. P., Colloidal Nanocrystal Synthesis and the Organic–Inorganic Interface. *Nature* **2004**, *437*, 664.
- 2. Wang, Y.; Zhou, Y.; Zhang, Y.; Buhro, W. E., Magic-Size II–VI Nanoclusters as Synthons for Flat Colloidal Nanocrystals. *Inorg. Chem.* **2015**, *54*, 1165-1177.
- 3. Carbone, L.; Nobile, C.; De Giorgi, M.; Sala, F. D.; Morello, G.; Pompa, P.; Hytch, M.; Snoeck, E.; Fiore, A.; Franchini, I. R.; Nadasan, M.; Silvestre, A. F.; Chiodo, L.; Kudera, S.; Cingolani, R.; Krahne, R.; Manna, L., Synthesis and Micrometer-Scale Assembly of Colloidal CdSe/CdS Nanorods Prepared by a Seeded Growth Approach. *Nano Lett.* **2007**, *7*, 2942-2950.
- 4. Puzder, A.; Williamson, A. J.; Zaitseva, N.; Galli, G.; Manna, L.; Alivisatos, A. P., The Effect of Organic Ligand Binding on the Growth of CdSe Nanoparticles Probed by Ab Initio Calculations. *Nano Lett.* **2004**, *4*, 2361-2365.
- 5. Wang, W.; Banerjee, S.; Jia, S.; Steigerwald, M. L.; Herman, I. P., Ligand Control of Growth, Morphology, and Capping Structure of Colloidal CdSe Nanorods. *Chem. Mater.* **2007**, *19*, 2573-2580.
- 6. Nasilowski, M.; Mahler, B.; Lhuillier, E.; Ithurria, S.; Dubertret, B., Two-Dimensional Colloidal Nanocrystals. *Chem. Rev.* **2016**, *116*, 10934-10982.
- 7. Ithurria, S.; Tessier, M. D.; Mahler, B.; Lobo, R. P. S. M.; Dubertret, B.; Efros, A. L., Colloidal Nanoplatelets with Two-Dimensional Electronic Structure. *Nat. Mat.* **2011**, *10*, 936.
- 8. Tessier, M. D.; Mahler, B.; Nadal, B.; Heuclin, H.; Pedetti, S.; Dubertret, B., Spectroscopy of Colloidal Semiconductor Core/Shell Nanoplatelets with High Quantum Yield. *Nano Lett.* **2013**, *13*, 3321-3328.
- 9. Scott, R.; Heckmann, J.; Prudnikau, A. V.; Antanovich, A.; Mikhailov, A.; Owschimikow, N.; Artemyev, M.; Climente, J. I.; Woggon, U.; Grosse, N. B.; Achtstein, A. W., Directed Emission of CdSe Nanoplatelets Originating from Strongly Anisotropic 2D Electronic Structure. *Nat. Nano.* **2017**, *12*, 1155.
- 10. Gao, Y.; Weidman, M. C.; Tisdale, W. A., CdSe Nanoplatelet Films with Controlled Orientation of Their Transition Dipole Moment. *Nano Lett.* **2017**, *17*, 3837-3843.

- 11. She, C.; Fedin, I.; Dolzhnikov, D. S.; Demortière, A.; Schaller, R. D.; Pelton, M.; Talapin, D. V., Low-Threshold Stimulated Emission Using Colloidal Quantum Wells. *Nano Lett.* **2014**, *14*, 2772-2777.
- 12. Guzelturk, B.; Pelton, M.; Olutas, M.; Demir, H. V., Giant Modal Gain Coefficients in Colloidal II–VI Nanoplatelets. *Nano Lett.* **2019**, *19*, 277-282.
- 13. Brütting, W.; Frischeisen, J.; Schmidt, T. D.; Scholz, B. J.; Mayr, C., Device Efficiency of Organic Light-Emitting Diodes: Progress by Improved Light Outcoupling. *Phys. Status Solidi A* **2013**, *210*, 44-65.
- 14. Saxena, K.; Jain, V. K.; Mehta, D. S., A Review on the Light Extraction Techniques in Organic Electroluminescent Devices. *Opt. Mater.* **2009**, *32*, 221-233.
- 15. Wang, Y.; Zhang, Y.; Wang, F.; Giblin, D. E.; Hoy, J.; Rohrs, H. W.; Loomis, R. A.; Buhro, W. E., The Magic-Size Nanocluster (CdSe)₃₄ as a Low-Temperature Nucleant for Cadmium Selenide Nanocrystals; Room-Temperature Growth of Crystalline Quantum Platelets. *Chem. Mater.* **2014**, *26*, 2233-2243.
- 16. Ithurria, S.; Dubertret, B., Quasi 2D Colloidal CdSe Platelets with Thicknesses Controlled at the Atomic Level. *J. Am. Chem. Soc.* **2008**, *130*, 16504-16505.
- 17. Joo, J.; Son, J. S.; Kwon, S. G.; Yu, J. H.; Hyeon, T., Low-Temperature Solution-Phase Synthesis of Quantum Well Structured CdSe Nanoribbons. *J. Am. Chem. Soc.* **2006**, *128*, 5632-5633.
- 18. Yu, J. H.; Liu, X.; Kweon, K. E.; Joo, J.; Park, J.; Ko, K.-T.; Lee, D. W.; Shen, S.; Tivakornsasithorn, K.; Son, J. S.; Park, J.-H.; Kim, Y.-W.; Hwang, G. S.; Dobrowolska, M.; Furdyna, J. K.; Hyeon, T., Giant Zeeman Splitting in Nucleation-Controlled Doped CdSe:Mn²⁺ Quantum Nanoribbons. *Nat. Mat.* **2009**, *9*, 47.
- 19. Son, J. S.; Wen, X.-D.; Joo, J.; Chae, J.; Baek, S.-i.; Park, K.; Kim, J. H.; An, K.; Yu, J. H.; Kwon, S. G.; Choi, S.-H.; Wang, Z.; Kim, Y.-W.; Kuk, Y.; Hoffmann, R.; Hyeon, T., Large-Scale Soft Colloidal Template Synthesis of 1.4 nm Thick CdSe Nanosheets. *Angew. Chem. Int. Ed.* **2009**, *48*, 6861-6864.
- 20. Liu, L.; Karuturi, S. K.; Su, L. T.; Tok, A. I. Y., TiO₂ Inverse-Opal Electrode Fabricated by Atomic Layer Deposition for Dye-Sensitized Solar Cell Applications. *Energy Environ. Sci.* **2011**, *4*, 209-215.
- 21. Liu, Y.-H.; Wayman, V. L.; Gibbons, P. C.; Loomis, R. A.; Buhro, W. E., Origin of High Photoluminescence Efficiencies in CdSe Quantum Belts. *Nano Lett.* **2010**, *10*, 352-357.
- 22. Wang, F.; Wang, Y.; Liu, Y.-H.; Morrison, P. J.; Loomis, R. A.; Buhro, W. E., Two-Dimensional Semiconductor Nanocrystals: Properties, Templated Formation, and Magic-Size Nanocluster Intermediates. *Acc. Chem. Res.* **2015**, *48*, 13-21.
- 23. Morrison, P. J.; Loomis, R. A.; Buhro, W. E., Synthesis and Growth Mechanism of Lead Sulfide Quantum Platelets in Lamellar Mesophase Templates. *Chem. Mater.* **2014**, *26*, 5012-5019.
- 24. Nevers, D. R.; Williamson, C. B.; Savitzky, B. H.; Hadar, I.; Banin, U.; Kourkoutis, L. F.; Hanrath, T.; Robinson, R. D., Mesophase Formation Stabilizes High-Purity Magic-Sized Clusters. *J. Am. Chem. Soc.* **2018**, *140*, 3652-3662.
- 25. Hsieh, T.-E.; Yang, T.-W.; Hsieh, C.-Y.; Huang, S.-J.; Yeh, Y.-Q.; Chen, C.-H.; Li, E. Y.; Liu, Y.-H., Unraveling the Structure of Magic-Size (CdSe)₁₃ Cluster Pairs. *Chem. Mater.* **2018**, *30*, 5468-5477.

- 26. Riedinger, A.; Ott, F. D.; Mule, A.; Mazzotti, S.; Knusel, P. N.; Kress, S. J. P.; Prins, F.; Erwin, S. C.; Norris, D. J., An Intrinsic Growth Instability in Isotropic Materials Leads to Quasi-Two-Dimensional Nanoplatelets. *Nat Mater* **2017**, *16*, 743-748.
- 27. Ott, F. D.; Riedinger, A.; Ochsenbein, D. R.; Knüsel, P. N.; Erwin, S. C.; Mazzotti, M.; Norris, D. J., Ripening of Semiconductor Nanoplatelets. *Nano Lett.* **2017**, *17*, 6870-6877.
- 28. Ithurria, S.; Bousquet, G.; Dubertret, B., Continuous Transition from 3D to 1D Confinement Observed During the Formation of CdSe Nanoplatelets. *J. Am. Chem. Soc.* **2011**, *133*, 3070-3077.
- 29. Liu, Y.; Zhang, B.; Fan, H.; Rowell, N.; Willis, M.; Zheng, X.; Che, R.; Han, S.; Yu, K., Colloidal CdSe 0-Dimension Nanocrystals and Their Self-Assembled 2-Dimension Structures. *Chem. Mater.* **2018**, *30*, 1575-1584.
- 30. Chen, Y.; Chen, D.; Li, Z.; Peng, X., Symmetry-Breaking for Formation of Rectangular CdSe Two-Dimensional Nanocrystals in Zinc-Blende Structure. *J. Am. Chem. Soc.* **2017**, *139*, 10009-10019.
- 31. Hines, M. A.; Guyot-Sionnest, P., Bright UV-Blue Luminescent Colloidal ZnSe Nanocrystals. *J. Phys. Chem. B* **1998**, *102*, 3655-3657.
- 32. Chen, H.-S.; Lo, B.; Hwang, J.-Y.; Chang, G.-Y.; Chen, C.-M.; Tasi, S.-J.; Wang, S.-J. J., Colloidal ZnSe, ZnSe/ZnS, and ZnSe/ZnSeS Quantum Dots Synthesized from ZnO. *J. Phys. Chem. B* **2004**, *108*, 17119-17123.
- 33. Wang, A.; Shen, H.; Zang, S.; Lin, Q.; Wang, H.; Qian, L.; Niu, J.; Song Li, L., Bright, Efficient, and Color-Stable Violet ZnSe-Based Quantum Dot Light-Emitting Diodes. *Nanoscale* **2015**, *7*, 2951-2959.
- 34. Shen, H.; Wang, H.; Li, X.; Niu, J. Z.; Wang, H.; Chen, X.; Li, L. S., Phosphine-Free Synthesis of High Quality ZnSe, ZnSe/ZnS, and Cu-, Mn-Doped ZnSe Nanocrystals. *Dalton Trans.* **2009**, 10534-10540.
- 35. Yeh, C.-Y.; Lu, Z. W.; Froyen, S.; Zunger, A., Zinc-Blende--Wurtzite Polytypism in Semiconductors. *Phys. Rev. B* **1992**, *46*, 10086-10097.
- 36. Panda, A. B.; Acharya, S.; Efrima, S., Ultranarrow ZnSe Nanorods and Nanowires: Structure, Spectroscopy, and One-Dimensional Properties. *Adv. Mater.* **2005**, *17*, 2471-2474.
- 37. Cozzoli, P. D.; Manna, L.; Curri, M. L.; Kudera, S.; Giannini, C.; Striccoli, M.; Agostiano, A., Shape and Phase Control of Colloidal ZnSe Nanocrystals. *Chem. Mater.* **2005**, *17*, 1296-1306.
- 38. Coropceanu, I.; Rossinelli, A.; Caram, J. R.; Freyria, F. S.; Bawendi, M. G., Slow-Injection Growth of Seeded CdSe/CdS Nanorods with Unity Fluorescence Quantum Yield and Complete Shell to Core Energy Transfer. *ACS Nano* **2016**, *10*, 3295-3301.
- 39. Jia, G.; Banin, U., A General Strategy for Synthesizing Colloidal Semiconductor Zinc Chalcogenide Quantum Rods. *J. Am. Chem. Soc.* **2014**, *136*, 11121-11127.
- 40. Ning, J.; Liu, J.; Levi-Kalisman, Y.; Frenkel, A. I.; Banin, U., Controlling Anisotropic Growth of Colloidal ZnSe Nanostructures. *J. Am. Chem. Soc.* **2018**, *140*, 14627-14637.
- 41. Park, H.; Chung, H.; Kim, W., Synthesis of Ultrathin Wurtzite ZnSe Nanosheets. *Mater. Lett.* **2013**, *99*, 172-175.
- 42. Zhang, L.-J.; Shen, X.-C.; Liang, H.; Yao, J.-T., Multiple Families of Magic-Sized ZnSe Quantum Dots Via Noninjection One-Pot and Hot-Injection Synthesis. *J. Phys. Chem. C* **2010**, *114*, 21921-21927.
- 43. Cui, J.; Beyler, A. P.; Coropceanu, I.; Cleary, L.; Avila, T. R.; Chen, Y.; Cordero, J. M.; Heathcote, S. L.; Harris, D. K.; Chen, O.; Cao, J.; Bawendi, M. G., Evolution of the Single-

- Nanocrystal Photoluminescence Linewidth with Size and Shell: Implications for Exciton—Phonon Coupling and the Optimization of Spectral Linewidths. *Nano Lett.* **2016**, *16*, 289-296.
- 44. Ithurria, S.; Talapin, D. V., Colloidal Atomic Layer Deposition (c-ALD) Using Self-Limiting Reactions at Nanocrystal Surface Coupled to Phase Transfer between Polar and Nonpolar Media. *J. Am. Chem. Soc.* **2012**, *134*, 18585-18590.
- 45. Evans, C. M.; Love, A. M.; Weiss, E. A., Surfactant-Controlled Polymerization of Semiconductor Clusters to Quantum Dots through Competing Step-Growth and Living Chain-Growth Mechanisms. *J. Am. Chem. Soc.* **2012**, *134*, 17298-17305.
- 46. García-Rodríguez, R.; Hendricks, M. P.; Cossairt, B. M.; Liu, H.; Owen, J. S., Conversion Reactions of Cadmium Chalcogenide Nanocrystal Precursors. *Chem. Mater.* **2013**, *25*, 1233-1249.
- 47. Murray, C. B.; Norris, D. J.; Bawendi, M. G., Synthesis and Characterization of Nearly Monodisperse CdE (E = Sulfur, Selenium, Tellurium) Semiconductor Nanocrystallites. *J. Am. Chem. Soc.* **1993**, *115*, 8706-8715.
- 48. Talapin, D. V.; Rogach, A. L.; Haase, M.; Weller, H., Evolution of an Ensemble of Nanoparticles in a Colloidal Solution: Theoretical Study. *J. Phys. Chem. B* **2001**, *105*, 12278-12285.
- 49. Beecher, A. N.; Yang, X.; Palmer, J. H.; LaGrassa, A. L.; Juhas, P.; Billinge, S. J. L.; Owen, J. S., Atomic Structures and Gram Scale Synthesis of Three Tetrahedral Quantum Dots. *J. Am. Chem. Soc.* **2014**, *136*, 10645-10653.
- 50. Wang, L.; Hui, J.; Tang, J.; Rowell, N.; Zhang, B.; Zhu, T.; Zhang, M.; Hao, X.; Fan, H.; Zeng, J.; Han, S.; Yu, K., Precursor Self-Assembly Identified as a General Pathway for Colloidal Semiconductor Magic-Size Clusters. *Adv. Sci.* **2018**, *5*, 1800632.
- 51. Zanella, M.; Abbasi, A. Z.; Schaper, A. K.; Parak, W. J., Discontinuous Growth of II–VI Semiconductor Nanocrystals from Different Materials. *J. Phys. Chem. C* **2010**, *114*, 6205-6215.
- 52. Luan, C.; Tang, J.; Rowell, N.; Zhang, M.; Huang, W.; Fan, H.; Yu, K., Four Types of Cdte Magic-Size Clusters from One Prenucleation Stage Sample at Room Temperature. *J. Phys. Chem. Lett.* **2019**, *10*, 4345-4353.
- 53. De Yoreo, J. J.; Vekilov, P. G., Principles of Crystal Nucleation and Growth. *Rev. Mineral. Geochem* **2003**, *54*, 57-93.
- 54. Chen, J.; Zhu, E.; Liu, J.; Zhang, S.; Lin, Z.; Duan, X.; Heinz, H.; Huang, Y.; De Yoreo, J. J., Building Two-Dimensional Materials One Row at a Time: Avoiding the Nucleation Barrier. *Science* **2018**, *362*, 1135-1139.
- 55. Glassy, B. A.; Cossairt, B. M., Ternary Synthesis of Colloidal Zn₃P₂ Quantum Dots. *Chem. Commun.* **2015**, *51*, 5283-5286.